

# Improvement in Cytoarchitectonic Mapping by Combining ElectrodynamiC Modeling With Local Orientation in High-Resolution Images of the Cerebral Cortex

OLIVER SCHMITT<sup>1</sup> AND HARALD BIRKHOLZ<sup>2</sup>

<sup>1</sup>Department of Anatomy, University of Rostock, 18055 Rostock, Germany

<sup>2</sup>Institute for Mathematics, University of Rostock, 18051 Rostock, Germany

**KEY WORDS** cerebral cortex; brainmapping; neuroimaging; parcellation; traverses; transcortical scanning; local orientation; coherence; anisotropic diffusion; electric field

**ABSTRACT** To detect changes of cortical cytoarchitectonics, digital images of cortical laminations are analyzed. Cortical regions are transformed into a rectangular grid for subsequent evaluations. Transformations are realized by stepwise scanning using perpendicular testlines. 3D cytoarchitectonic data of the human brain at a histological resolution are not available and 2D sections deliver partial information only. The problem is to find an optimal scanning-technique that introduces a minimum of distortions and noise by the transformation of the curvilinear cortex to a rectangular presentation. In the past this was solved by constructing testlines dependent on the outlined cortical contours only. An advanced approach was to model the contours as electrically charged surfaces and to use the resulting field lines as testlines. However, local information of cell distributions were not considered. Hence a novel hybrid approach was developed which is able to construct significantly better testlines in cortical images with mixtures of columnar rich (local orientation rich) and orientation poor parts of strongly curved and large regions of the cerebral cortex. The novel hybrid approach is based on the computer vision methods such as the structure tensor and constrained anisotropic diffusion. In addition, the introduction of projective transformations yields a significant improvement of cortical fingerprints, thereby offering the possibility for detecting weakly pronounced regions of cytoarchitectonic transitions. The statistical evaluation of the novel hybrid approach confirms robustness. This technique can be generalized and applied to different types of cerebral cortex with any kind and amount of local orientation information. *Microsc. Res. Tech.* 74:225–243, 2011. © 2010 Wiley-Liss, Inc.

## INTRODUCTION

The human cerebral cortex is comparable with a topological envelope of gray matter covering a core of white matter. This gray matter of the cortical mantle is not a uniform layer of neurons and supporting cells. It is striped by a distinct internal lamination determined genetically (Chambers and Fishell, 2006; Mallamaci and Stoykova, 2006), which varies locally and can be subdivided by different parcellation schemes based on visualizations like cyto-, myelo-, pigment- or angioarchitectonics (Braak, 1980; Brodmann, 1909; Campbell, 1905; Elliot Smith, 1907; Pfeifer, 1940; von Economo and Koskinas; Vogt and Vogt, 1919, 1925) as well as receptorarchitectonics (Zilles and Palomero-Gallagher, 2001; Zilles et al., 1995, 2004) and chemoarchitectonics (Borostyankoi-Baldauf and Herczeg, 2002; Jacobowitz et al., 2004; Mitrofanis et al., 2004; Rosano et al., 2003). Functional mapping (Huettel et al., 2004; Toga, 2002) and chronoarchitectonics (Bartels and Zeki, 2005) are investigated *in vivo* by high resolution fMRI. As a great advance, MRI and fMRI data were correlated with high resolution structural postmortem data (Amunts and Zilles, 2001; Choi et al.,

2006; Mazziotta et al., 2001; Roland and Zilles, 1998; Roland et al., 1997).

In the merits using conventional methods, parcellation was done subjectively, which was heavily criticized (Baily and von Bonin, 1951; Lashley and Clark, 1946). Furthermore, intersubject variability (Amunts et al., 1999a, 2000b; Filimonoff, 1932; Geyer et al., 1996, 1999; Roland and Zilles, 1998; Roland et al., 1997) was not taken into consideration. The printed 2D-maps were worked out on different projections and unfolding schemes resulting in highly schematic drawings. Hence, they do not provide spatial information necessary for studies of spatio-temporal structure function correlations (Amunts et al., 2000a; Eickhoff et al., 2005; Walters et al., 2006).

In pioneering investigations of Hopf (1966, 1968b,a) and Hudspeth et al. (1976), density profiles running

\*Correspondence to: Oliver Schmitt, Department of Anatomy, University of Rostock, 18055 Rostock, Germany. E-mail: schmitt@med.uni-rostock.de

Received 1 February 2010; accepted in revised form 28 May 2010

Abbreviations: 2D, two dimensional; 3D, three dimensional; ED, electrodynamiC approach; EDT, electrodynamiC traverses; fMRI, functional magnetic resonance imaging; HD, hybrid diffusion approach; HT, hybrid traverses; HY, hybrid approach; IT, ideal traverses; MRI, magnetic resonance imaging; ODE, ordinary differential equations; PDE, partial differential equations; resp., respectively; ROI, region of interest; S.E.M., standard error of mean.

DOI 10.1002/jemt.20897

Published online 4 August 2010 in Wiley Online Library (wileyonlinelibrary.com).

perpendicular to the cortical layers to quantify the lamination pattern were elaborated. Schleicher et al. (1978) were the first who developed algorithms for an observer-independent approach, which was improved further on (Schleicher and Zilles, 1990; Schleicher et al., 1999, 2000, 2005) to quantify cortical lamination and to compare statistically different lamination patterns. First, linear traverses were calculated based on the construction of perpendicular lines on a centerline and adaption with regard to their intersections with other traverses. These traverses are testlines oriented almost perpendicular to the cortical lamination. Using the path of a traverse pixel intensities in the digitized image of a stained brain section can be determined and transformed as a profile. The profile pattern or fingerprint needs to be analyzed statistically (Schleicher et al., 1999, 2000; Schmitt et al., 2003, 2004) to determine transition zones observer independently.

Cortical layering is a phenomenon that originates from a stripe-like spatio-temporal clustering of neurons within corticogenesis (Feng et al., 2000; Hevner et al., 2003; Rakic, 1988). Most of the cortical layers run parallel between the pial surface and the white matter border. The derived profiles should be oriented perpendicular to the layers which are curved due to cortical folding. If the traverses are not consistently perpendicular to the cortical lamination, or if they intersect, the resulting intensity profiles will be distorted and will contain high levels of noise. As mentioned above, layering emerges from the phenomenon of stripe-like clustering of neurons running parallel to the pial surface. This is an important local feature of the cerebral cortex. Therefore, the accuracy of calculation of the local layer dependent perpendicularity strongly depends on detection of such local features like stripes and columns, resp. minicolumns or microcolumns (Buxhoeveden et al., 2000; Casanova et al., 2007; Horton and Adams, 2005; Mountcastle, 1997) in between lamina II and lamina VI. Such minicolumns contain 90–100 neurons and have a diameter of 20–60  $\mu\text{m}$  with an intercolumnar distance of 80  $\mu\text{m}$ . Minicolumns are bound together by short-range horizontal connections building macrocolumns (=hypercolumn of the visual cortex) of 60 to 80 minicolumns. Estimating the path of a curvilinear traverse by considering solely the external and internal boundary of the cerebral cortex seems to be an appropriate approximation; however, it could fail if layers do not follow exactly parallel to the external and internal cortical borders. The latter situation occurs rather often in variable degree and gains additional importance with regard to tangential or oblique sectioning of parts of the cortical lamination.

The cortical ribbon is not homogeneous internally but constitutes a highly complex radial and tangential internal structural framework. The effect of curvature on the internal and external surface of the cerebral cortex was predicted by Bok (1959) on theoretical grounds and further studied empirically by Smart and McSherry (1986a,b) in the developing brain of the ferret. In these studies, merely surfaces were considered; however, they emphasize that the cortical layers are subject to considerable geometrical distortion during gyrogenesis as indicated by the change in the curvature and direction of radial lines.

A 3D artificial cortical cytoarchitecture has been calculated to demonstrate the effects of oblique sectioning

(Fig. 1). The model consists of six layers (green cells) and nine columns (red cells). Cell densities of the layers have been estimated and noise (blue cells) has been added. From an ideal orthogonal section, a profile has been calculated (Fig. 1b). The oblique section in Figure 1d leads to strong distortions of the profile pattern (Figs. 1e, f). More or less strong nonorthogonal sections need to be evaluated (Fig. 1g) to generate profile arrays that should be calculated optimal with regard to the course of cortical layers. Then, a characteristic profile can be determined containing a minimum of disturbances.

Therefore, we developed an approach based on applying the electric field model considering the external and internal border of the cerebral cortex (De Vos 1999, personal communication; Schmitt and Böhme, 2002) by solving ordinary differential equations and the local orientation (Bigün and Granlund, 1987; Granlund and Knutson, 1995; Schmitt et al., 2004) of neuron and other cell distributions to generate curvilinear traverses running locally perpendicular to the cortical layering. A second improvement was realized by using a new sampling technique based on projective transformation. Third, the local orientation computation was supported by a new local anisotropic diffusion scheme (Perona and Malik, 1990; Weickert, 1998, 1999) to enhance selectively those cell distributions that contribute to preferential orientations perpendicular to the borders of the cerebral cortex, like minicolumns. An important feature of this technique is that it makes use of the coherence of local orientation for weighting local orientation, and the electrodynamic approach controlled by the incomplete Beta-function. This has the great advantage that those parts of the cerebral cortex that do not show columns or contain structural disturbances of columns due to shrinkage caused by paraffin embedding (columns are moving together) and non orthogonal sectioning still can be analyzed optimally because the electrodynamic part of the hybrid approach is weighted stronger. Furthermore, such a dynamic behavior of the algorithm is important because the morphological expression of vertical columns in different cortical areas is unknown: some regions tend to be more columnar than others, in the visual cortex columns are larger than in other areas, a columnar lateralization is known and interspecies differences exist (Buxhoeveden and Casanova, 2002). The new hybrid approach was compared to traverse paths (ideal traverses) outlined interactively by experienced experts in cytoarchitectonic analysis. Then, it was analyzed with regard to different types of curvature of ROIs of cortical images and evaluated statistically. Finally, an optimal set of parameters used by the new hybrid approach for a reliable sampling of the cortical ribbon is suggested.

In the following three parts of this article, the methods, results, and discussion are organized with subsections. The methods part begins with basic definitions, conditions, and an introduction of the structure-tensor. The coherence is defined with respect to the eigenvalues of the structure tensor. Then, the incomplete Beta-function is applied to smoothly threshold the coherence. In the second subsection, the hybrid approach that connects the electrodynamic technique with the local orientation approach is presented. In the third subsection, the anisotropic diffusion is introduced to

enhance local orientation of the cytoarchitectonic data domain. The process of traverse calculation is described, too. The combination of the hybrid method with an orientation enhancement by the anisotropic diffusion results in a new powerful strategy leading to statistically significant superior results which are presented in the results part. As a further advance, we introduce the piecewise projective transformation to calculate cortical fingerprints profiles. The last subsection of the methods part addresses the procedure for comparing the three techniques electrodynamic (ED), hybrid (HY), and hybrid diffusion (HD) by an error measure  $\alpha$ . In the results part, we are beginning with the visualization of the ED and HD followed by the quality measurement, statistic comparison, and the exploration of optimal parameters for HY and HD. Several technical and cytoarchitectonic aspects are critically pointed out in the discussion closing with new ideas for the further development of the HY and HD methods with partial differential methods in three dimensions.

## MATERIAL AND METHODS

This section treats mainly the new ideas on the traverse generation problem for neuronal stained cortex images. The key idea is the use of the image for steering the sampling process. The former electrodynamic model based on the time integration of a system of ODEs is augmented by a modification of the force field. The modification is given by weighted averaging of an electrodynamic part and a vector which estimates the direction of neural columns in a neighborhood of the traverse at the image. Neural columns are modeled as locations in the image in which the image shows great smoothness into one direction and great variation perpendicular. The estimation of neural columns is, therefore, realized with the tensor representation of local orientation. In this matrix-valued feature, the eigenvector of the smallest eigenvalue points in the direction of least gray-value variation or greatest local smoothness. Almost equal eigenvalues occur and interfere with well-posedness of the initial-value problem of the system of ODEs. This problem is avoided by using the enhanced coherence, essentially the difference of the eigenvalues, as the weighting factor of local orientation in the driving force field. With the integration of the force-field, traverses are generated, which run perpendicularly into the boundary of the ROI and tend to run parallel to neural columns inside the ROI. For their computation, a charge is placed near the boundary inside the ROI and moved to the opposite boundary by the force. A preprocess with coherence-enhancing diffusion allows for a further improvement of the adaptivity behavior. It amplifies the pointers to neural columns by blurring the random background information and, thus, reducing inconsistencies of the local orientation estimation.

### Histological Sections and Digitizing

For testing and comparing, the new approach 20  $\mu\text{m}$  thick human brain sections stained with a silver staining (Merker, 1983) are used. Stained sections are digitized using the high-resolution transparent flatbed scanner NEXSCAN F4100 (Heidelberger) providing a resolution of 5.04  $\mu\text{m}$  per pixel with an 8 Bit dynamic.

## Motivation and Notation

These 2D (scalar-valued) images are modeled by the continuous function  $f: \mathbb{R}^2 \rightarrow \mathbb{R}$  with compact support. An image is supplemented with a manually defined region of interest  $\Omega \subset \mathbb{R}^2$  with topological gender 0 or 1. For the ease of notation, we restrict to the first case. The ROI is the area between two contours  $H, L \subset \partial\Omega$ , which represent the boundary of the gray matter with the surrounding tissue. To cope with the geometry of  $\Omega$ , traverses are computed. They define a transformation of  $f|_{\Omega}$  into a cortical fingerprint.

Traverses should exhibit the following properties:

1. A traverse is a curve from  $H$  to  $L$ .
2. Different traverses do not intersect.
3. Traverses cross the layers of the gray matter locally orthogonal.

The properties (1) and (2) are achieved with the electrodynamic model (Schmitt and Böhme, 2002). It entirely relies on the manually defined contours, which are modeled as electrically charged, inducing a force field that drives mobile charges across the ROI. The trace of a charge that starts near a contour is used as a traverse. This is computationally efficient and reliable. The problem is that the property (3) is only achieved for the outermost layers. For a given image, it is possible to stabilize the electrodynamic model against bias of manual input by including the image into the traverse generation algorithm to fulfill the property (3).

For an estimation of the orientation locally orthogonal to gray-matter layers, neural columns are estimated. Along these line-like structures,  $f$  is assumed to be smoother in comparison to the otherwise relatively random distribution and the distribution of neurons clustered in a multiple layer-like architecture in the ROI. Column-like anisotropic structures are superposed by isotropic and layer structures, whereby the latter are oriented quasi-parallel to the pial surface and the gray-matter border. With the structure-tensor, which is a gradient-based low-level feature, the anisotropy can be estimated. The estimation must be enhanced by thresholding to exclude random anisotropy that does not originate from neural columns.

We write for any  $M, N \in \mathbb{N}$  and any feature  $h \in L^1(\mathbb{R}^2, \mathbb{R}^{M \times N})$ :

$$h_{\sigma} := \begin{pmatrix} h_{11} * G_{\sigma} & \dots & h_{1N} * G_{\sigma} \\ \vdots & & \vdots \\ h_{M1} * G_{\sigma} & \dots & h_{MN} * G_{\sigma} \end{pmatrix}$$

with  $\sigma > 0$  and  $h_0 := h$ , where  $G_{\sigma}(x) = \frac{1}{2\pi\sigma^2} \exp(-\frac{\|x\|^2}{2\sigma^2})$  is a Gaussian kernel and  $*: L_1(\mathbb{R}^2) \times L_1(\mathbb{R}^2) \rightarrow L_1(\mathbb{R}^2)$  is the convolution. The feature  $h$  is smoothed to an extent  $\sigma$ . The spatial argument is omitted in the following formulas. All features are supposed to be pointwise eval-

uated. We write the structure-tensor  $J$  of an absolute integrable function  $u: \mathbb{R}^2 \rightarrow \mathbb{R}$  as

$$J := (\nabla u_\varepsilon (\nabla u_\varepsilon)^T)_\rho \quad \varepsilon, \rho \geq 0.$$

This is the outer product of a smoothed gradient  $\nabla u_\varepsilon$ , itself smoothed in each component. The matrix  $J$  is symmetric and positive semidefinite everywhere because  $\nabla u_\varepsilon (\nabla u_\varepsilon)^T$  has the nonnegative eigenvalues 0 and  $\|\nabla u_\varepsilon\|^2$ . By the linearity and monotonicity of the integral, the convolution with a positive Gaussian kernel preserves positive semidefiniteness, see also Weickert (1998). Let  $\lambda_1 \geq \lambda_2 \geq 0$  be the eigenvalues of  $J$  with eigenvectors  $v_1, v_2 \in \mathbb{R}^2$ . In case  $\lambda_1 > \lambda_2$ , the eigenvector  $v_1$  exposes the orientation of the greatest local gray-value variation. The vector  $v_2$  is orthogonal to  $v_1$  and, thus, indicates an orientation of greatest local smoothness of  $u$ . If  $\lambda_1 = \lambda_2$ , the eigenvectors of  $J$  are arbitrary and meaningless. Thus, the difference  $\lambda_1 - \lambda_2$  is a measure for the accuracy of the orientation estimation encoded in  $v_1$  and  $v_2$ . Inspired by Jähne (2004), it is used in a smoothly normalized form which is called coherence  $c$ :

$$c := \frac{\lambda_1 - \lambda_2}{\lambda_1 + \lambda_2 + \varepsilon}, \quad 0 < \varepsilon \ll 1.$$

The coherence  $c$  can be regarded as a probability for the assumption that the underlying image  $u$  shows column-like structures in a  $\rho$ -neighborhood. To make sure these elongated structures are neural columns,  $c$  is smoothly thresholded with the incomplete Beta-function. Its parameters shape is sigmoid as a function of  $c$ , with an inflection point at  $\theta \in [0, 1]$  and a slope  $s > 1$  at  $\theta$  (Fig. 2). The result provides a real number  $\beta$  that can be interpreted as a local probability of neural columns of width  $\sigma$  with a coherence greater than  $\theta$  to a  $\rho$ -neighborhood:

$$\beta := \frac{1}{B(\mu, \nu)} \int_0^\theta \xi^{\mu-1} (1-\xi)^{\nu-1} d\xi,$$

with  $\mu := s$  and  $\nu := \frac{(1-\theta)(s-1)}{\theta} + 1$  and  $B$  the Beta-function. Obviously,  $\beta \rightarrow 0$  as  $\theta$  approaches 1 provided  $s > 1$ . This will be important for the hybrid traverse generation model, see Section "Hybrid Electrodynamic Traverse Generation", because in this sense, it is a generalization of the electrodynamic model (Schmitt and Böhme, 2002). It must be emphasized that not in each region of the cerebral cortex proper cell orientations occur (i.e. cell columns perpendicular to the cortical surface). If the orientation is large enough, it will be strongly weighted and vice versa. From this follows that in oblique sections of the cerebral cortex exhibiting low or no perpendicular orientations of cells the contribution of the electrodynamic technique will be strong. Blood vessels, staining artifacts, and local damage of the sections typically result in low local orientation. Hence, the electrodynamic approach will prevail in these cases based on the inner and outer contours, which are not affected by this kind of noise.

Figure 3a visualizes  $\beta \equiv c$  reproducing the coherence at the ROI for  $\theta \in (0, 1)$  and  $s = 1$ . In Figure 3b the  $\beta$  distribution on  $\Omega$  for a non-trivial choice of parameters,  $\theta =$

0.2 and  $s = 16$  is shown. Plots of  $\beta$  as a function of  $c$  for (a) and (b), respectively, are shown in Figures 3c and 3d.

In Figure 4, the local orientations are plotted within the data domains (Figs 4a and 4b). The orientation is color coded according to the scheme in Figure 4b (inset). The orientation of the electrodynamic flow is shown in Figure 4a. The ED produces relatively similar orientations within straight parts of the cortex. However, the HY is sensitive to local changes of cell distributions and their local orientations. Therefore, straight parts of the cortex may show stronger changes of orientations.

### Hybrid Electrodynamic Traverse Generation

The curvilinear paths of traverses computed by the ED (Schmitt and Böhme, 2002) or alternative approaches (Schleicher and Zilles, 1990; Schleicher et al., 1999, 2000, 2005) do not necessarily achieve the condition (3) (see above) that they should be oriented locally perpendicular to cortical layers. As inner and outer contours contribute only partial data for determining local layer-specific orientation, we can use the concept of local orientation (Bigün and Granlund, 1987; Granlund and Knutson, 1995; Schmitt et al., 2004).

Cortical layering is complicated and extremely variable. As this approach should be generalizable for different types of cortical layering, it should work also in those regions, where the layering is blurred due to sectioning or where transitional zones occur. Cytoarchitectonic cell columns (Buxhoeveden et al., 2000; Casanova et al., 2007; Horton and Adams, 2005; Mountcastle, 1997) facilitate the determination of locally perpendicular traverses; however, they are not always visible due to tangential sectioning. In the case of low local coherence of orientation, the weight of the electrodynamic approach should increase and vice versa. Therefore, it seems reasonable to weight the electrodynamic technique and the local orientation to a hybrid electrodynamic orientation approach (HY).

The new traverse generation algorithm augments the electrodynamic model. Formerly, an electric field  $F: \mathbb{R}^2 \rightarrow \mathbb{R}^2$  drives charges one by one from the push contour  $H$  to the pull contour  $L$ , across  $\Omega$ :

$$F(x) := \int_H \frac{x - \xi}{\|x - \xi\|^3} d\xi + \int_L \frac{\xi - x}{\|\xi - x\|^3} d\xi.$$

For the electrodynamic model, the system of ODEs

$$\begin{aligned} \dot{y} &= \frac{F(y)}{\|F(y)\|}, \\ y(0) &= y_0^k, \\ y(t) &\in \Omega \end{aligned}$$

is solved for different  $y_0^k$  which are placed near the push-contour  $H$ . This results in curves similar to electrical field lines. They run into the contours orthogonally. However, the traverses exhibit an unsatisfying behavior in between. Therefore, the driving force of the charge is modified, so it moves preferably with the local orientation of neural columns, which we assume to exhibit a certain coherence. For this the structure tensor  $J$  of the image with eigenvalues  $\lambda_1 \geq \lambda_2 \geq 0$  is applied. The amplified

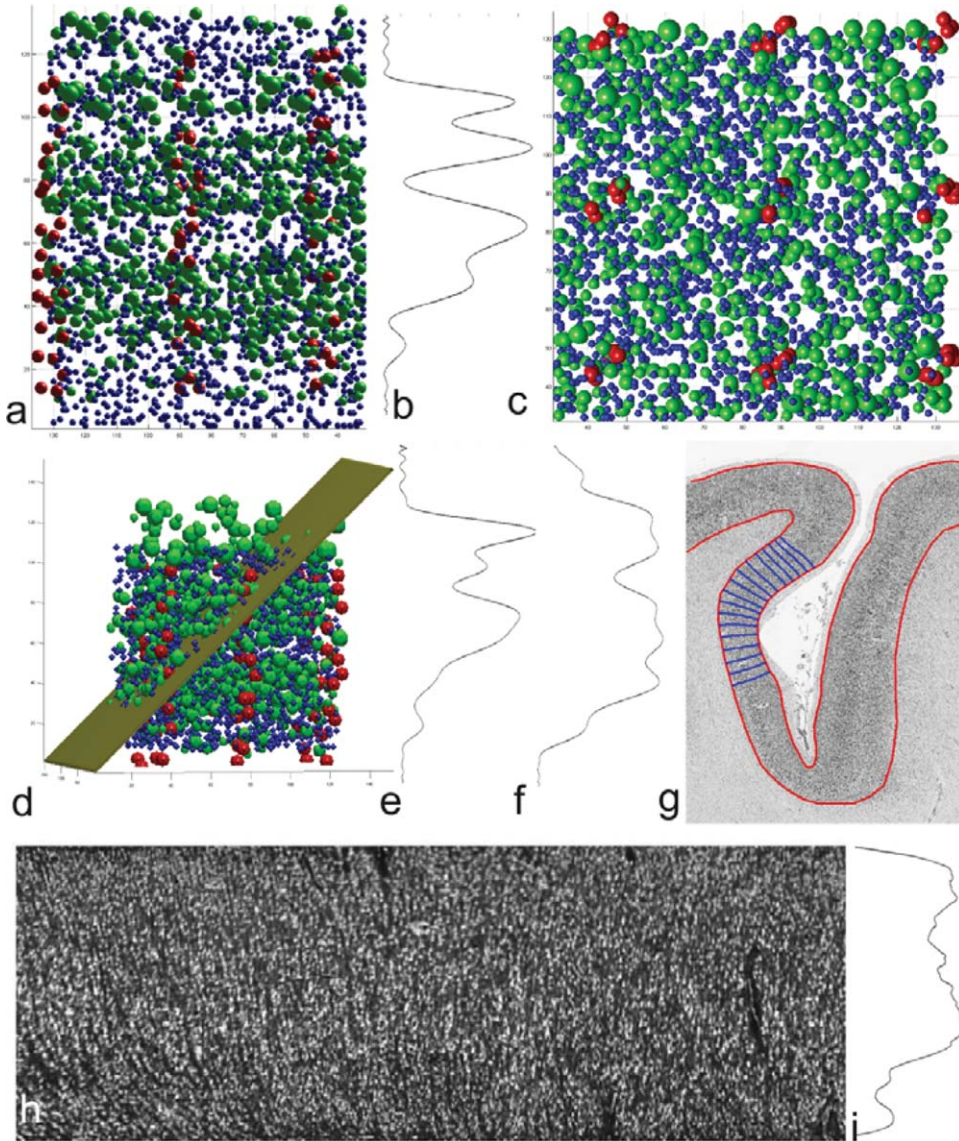


Fig. 1. **a:** Lateral view of a 3D cortical model. Layers 1–6 (green cells) and three columns (red cells) are visible. The profile of this view is shown in **(b)**. **c:** View from top where the nine minicolumns can be seen. **d:** Oblique section through the model. **e** and **f** are the resulting profiles of two different oblique sections. **g:** A typical isocortical

region in area 6 of a human brain where testlines were calculated and a profile array was generated **(h)**. **i:** Shows the characteristic profile with the typical cytoarchitectonic layering of area 6. [Color figure can be viewed in the online issue, which is available at [wileyonlinelibrary.com](http://wileyonlinelibrary.com).]

coherence is given by  $\beta$ , see Section “Motivation and Notation”. The crucial directional information in  $x \in \mathbb{R}^2$  is given by an eigenvector  $P(x)$  of  $J(x)$  to  $\lambda_2(x)$ , which encloses an acute angle with  $F(x)$ . Then, the traverse is created with a time integration of another system of ODEs. We solve:

$$\begin{aligned}\dot{y} &= \beta \frac{P(y)}{\|P(y)\|} + (1 - \beta) \frac{F(y)}{\|F(y)\|}, \\ y(0) &= y_0^k, \\ y(t) &\in \Omega.\end{aligned}$$

Let  $T_2$  be the time, when  $y$  reaches  $L$ , so that we can inductively define a family of traverses with length 1 by:

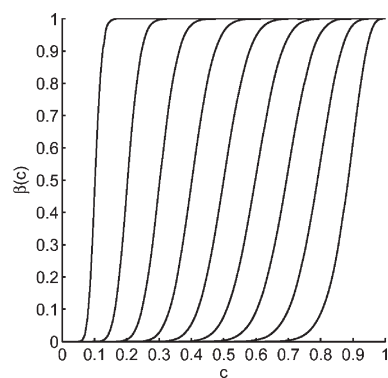


Fig. 2.  $\beta$  as a sigmoid function of  $c \in [0, 1]$  for  $\theta \in \{0.1, 0.2, \dots, 0.9\}$  and constant  $s = 16$ .

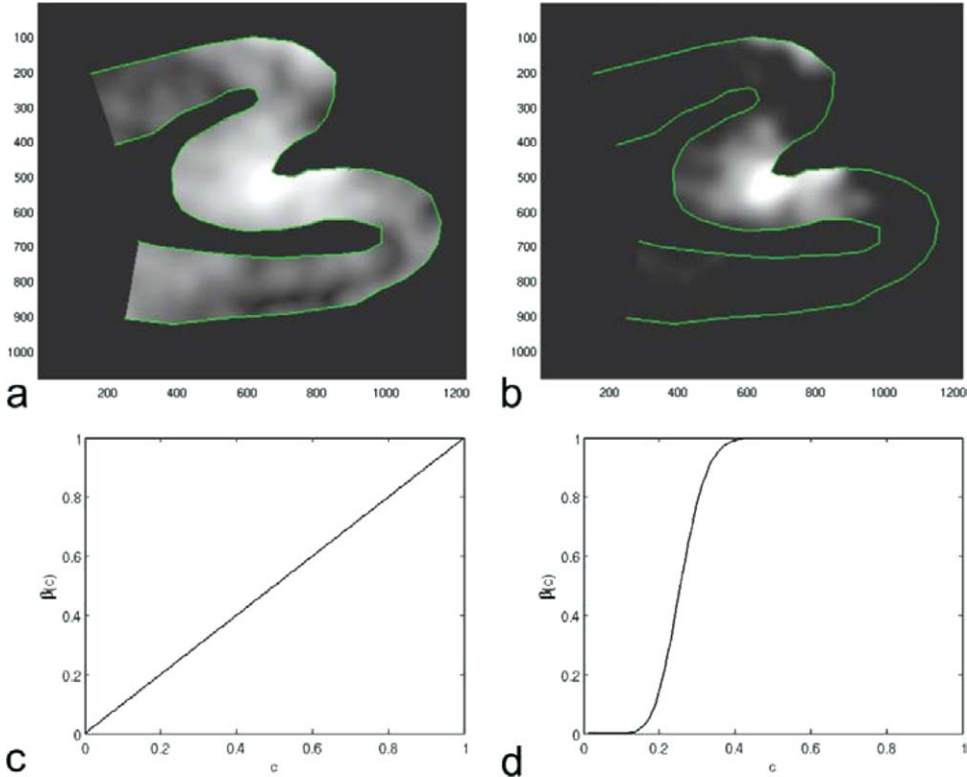


Fig. 3. (a) The coherence  $c$  as a special case of  $\beta$  with  $\theta \in (0,1)$  and  $s = 1$ . (b)  $\beta$  of the image function with  $\theta = 0.2$ ,  $s = 16$ . In (c) (for  $\beta$  with  $\theta \in (0, 1)$ ) and (d) (for  $\theta = 0.2$ ,  $s = 16$ ) the incomplete Beta-function for pointwise coherence enhancement is shown. [Color figure can be viewed in the online issue, which is available at [wileyonlinelibrary.com](http://wileyonlinelibrary.com).]

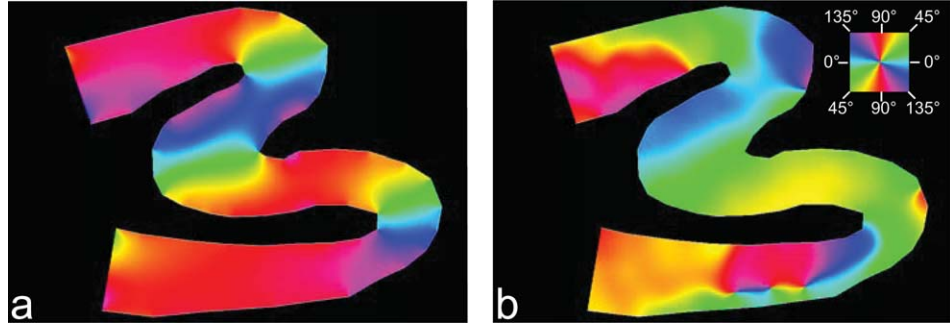


Fig. 4. (a) The local orientation of the electrodynamic flow and (b) of the structure-tensor of the hybrid method. The corresponding histograms of the estimated errors of angles between ideal and computed traverses are shown in Figure 7. [Color figure can be viewed in the online issue, which is available at [wileyonlinelibrary.com](http://wileyonlinelibrary.com).]

$$Y^k(t) := y(tT_2).$$

The traverses are decomposed by  $0 = t_0 < t_1 < \dots < t_n = 1$  into the grid of non degenerated quadrilaterals:

$$Y^{k,l} := Y^k(t_l),$$

provided the traverses are computed with an appropriate accuracy with respect to their density and  $n$  is great enough.

An appropriate sequence of computing the traverses is realized to keep the distortion by an area-preserving transformation of the grid meshes small. We start with the first

and the last path. Then, we densify the paths recursively. For this, we compute two paths per pair of adjacent paths. One starts from the inner contour, half way between the two. The other starts from the outer contour, half way between the two. We decide which one will be added to the set of paths by looking at which divides the area bounded by the two adjacent paths and the contours best into equal parts. Then, we go on with the same procedure for the old paths and their new neighbors, see Figure 5.

An implementation needs to evaluate  $F$  for given contours and  $P$  and  $\beta$  for given images at every location in  $\Omega$ . This is sufficiently provided by a routine that handles the influence of every contour segment and sliding windows of the image. Especially, the sliding windows

of the image for the structure-tensor evaluation are a bottleneck of a straightforward implementation. The evaluation of a smoothed gradient, its outer product, and an integration of a neighborhood for the three independent components are required. Although the first step consists of a convolution, the integration over a neighborhood suffices with a scalar-product with a window centred at an inter-pixel position. An interpolation of a structure tensor computed at the image grid in advance would also be possible. It might be advantageous if most pixels were closest to the site of evaluation at least twice, which is not the case for a reasonable step-size in the time-integration of the system of ODEs and a reasonably sparse spacing of traverses. In this setting, we used the variable order Adams-Bash-

forth-Moulton PECE solver ODE113 implemented in the technical computing software Matlab. It is recommended for costly right-hand-sides for taking advantage of preceding steps of the solution.

### Coherence-Enhancing Diffusion for Preprocessing

Anisotropic diffusion is a nonlinear filtering technique based on the numerical solution to the partial differential equation describing the process of diffusion. It is a space variant noise reduction technique that can selectively preserve texture, edges, and other details. The method is an efficient nonlinear filter for simultaneously performing contrast enhancement and noise reduction. It smoothes homogeneous image regions and retains image edges. The main concept of anisotropic diffusion is the diffusion coefficient (Perona, 1998; Perona and Malik, 1990).

The coherence of an image should be used for local orientation estimation. Therefore, it is self-evident to apply anisotropic diffusion filtering to enhance local orientation. The idea is to smooth an image first into the direction it already is smoothest. In the steady-state, there is an improvement of coherence. The visual impression of the intermediate results is flow like, and its value is twofold. First, any line-like structures are enhanced, so the existence is no longer in question. Second, the greater coherence might help to get a better estimation of the anisotropy in the ROI. We solve a slightly modified coherence-enhancing diffusion scheme, to be found in Weickert (1998):

$$\begin{aligned} u_t &= \nabla \cdot (D \nabla u) && \text{for } (t, x) \in (0, T_1) \times \Omega, \\ u(0, x) &= f(x) && \text{for } x \in \Omega, \end{aligned}$$

with the given image  $f(x)$  as initial condition and no flux across the boundary. The diffusivity  $D : \mathbb{R}^2 \rightarrow \mathbb{R}^{2 \times 2}$  is faithful to the common scheme with the slight modification that the flux is thresholded to enhance exclusively neural columns and leave other superposed structures untouched. Let

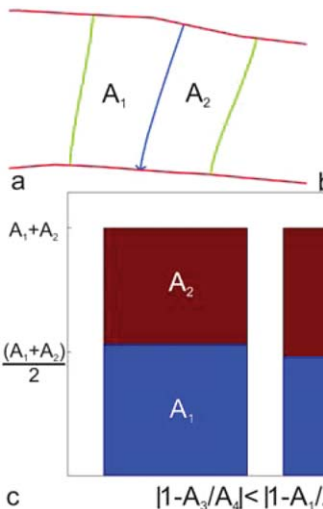


Fig. 5. **a:** Blue traverse starting from the upper contour half way between the end points of the green traverses. **b:** Blue traverse starting from the lower contour half way between the end points of the green traverses. **c:** The traverse that divides the area between the green neighboring traverses best into equal parts is selected and considered for eventual further densification. [Color figure can be viewed in the online issue, which is available at [wileyonlinelibrary.com](http://wileyonlinelibrary.com).]

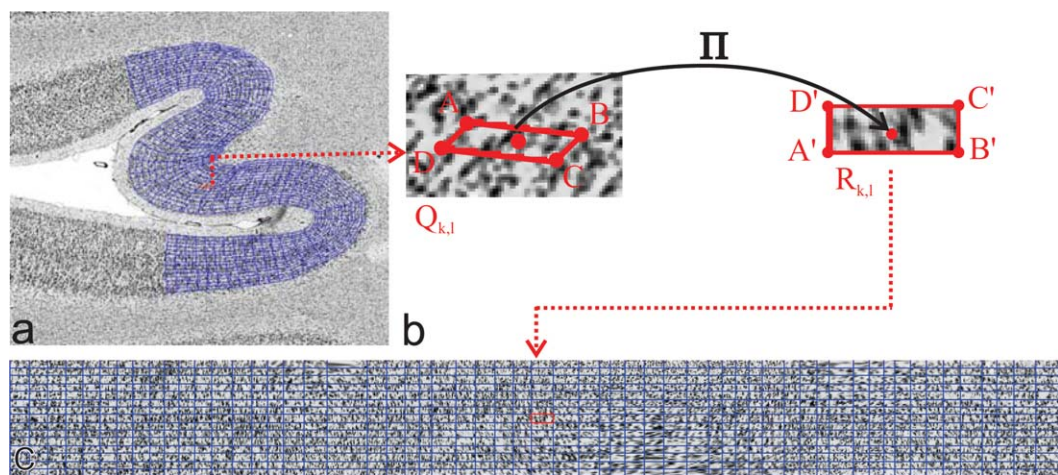


Fig. 6. The sampling is realized by projective mapping. A rectangle between the traverse paths is mapped to a grid mesh. [Color figure can be viewed in the online issue, which is available at [wileyonlinelibrary.com](http://wileyonlinelibrary.com).]

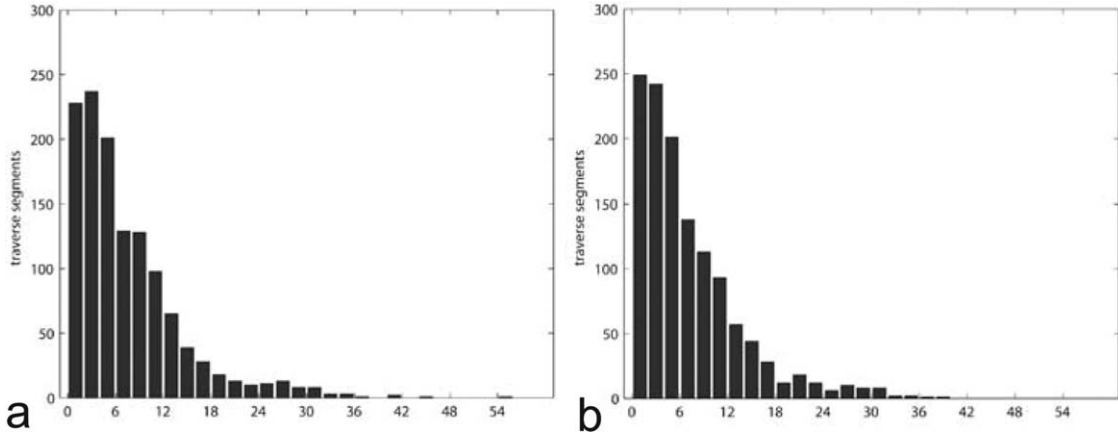


Fig. 7. **a:** The histogram of  $\{\varphi_{k,l}; (k,l) \in E\}$  for the ED and **(b)** for the hybrid model with diffusion pre-process HD (cf. Fig. 4).

$$J = Q \begin{pmatrix} \lambda_1 & \\ & \lambda_2 \end{pmatrix} Q^T, \quad Q \text{ orthogonal},$$

be the diagonalized structure tensor with  $\lambda_1 \geq \lambda_2 \geq 0$ . Then, we set

$$D := Q \begin{pmatrix} \mu_1 & \\ & \mu_2 \end{pmatrix} Q^T$$

with

$$\mu_1 := \varepsilon$$

$$\mu_2 := \begin{cases} \varepsilon & \text{for } \lambda_1 = \lambda_2 \\ \varepsilon + (1 - \varepsilon)\beta \exp\left(-\frac{1}{(\lambda_1 - \lambda_2)^2}\right) & \text{for } \lambda_1 \neq \lambda_2 \end{cases}$$

where  $0 < \varepsilon \ll 1$ .

With this construction of  $D$ , the initial value problem is well posed and delivers a unique solution for all stopping times  $T_1$ , see Weickert (1998). The most questionable part of the proof is the smoothness of  $D$  in  $J$ . This is ensured by the smoothness of  $\beta$  in  $J$ .

### Piecewise Projective Transformation

The derivation of the cortical fingerprint is the final purpose of the traverse computation. A direct approach is to read the pixels under each traverse and transfer them as a column into the fingerprint. This leads to a questionable sampling because the distance between traverses can vary, especially in strongly curved regions. Only one traverse at a time is used, discarding knowledge about their neighboring traverses. The new approach to the fingerprint extraction problem is a piecewise planar projective transformation from the traverse grid into a template grid. Let

$$Q_{k,l} \subset \mathbb{R}^2, \quad k = 0, \dots, m-1, l = 0, \dots, n-1$$

be the quadrilateral with the corners  $\{Y^{k,l}, Y^{k+1,l}, Y^{k,l+1}, Y^{k+1,l+1}\}$ . We assume that it is convex. The gray values of the image at  $Q_{k,l}$  are mapped to a template quadrilateral  $R_{k,l}$ , where  $R_{k,l}$  is part of a matrix of quadrilaterals which forms the fingerprint. The nodes of the template grid are chosen such that the area of

the grid meshes is well preserved. This is achieved with a width of  $R_{k,l}$  computed as the area between the contours and the traverses  $Y^k$  and  $Y^{k+1}$  divided by their average length. Accordingly, the height is chosen  $(Y^k + Y^{k+1})/(2n)$ . The mapping that we use for pairs of original and template quadrilaterals  $Q, R$ , is the unique planar projective transformation  $\Pi: Q \rightarrow R$ :

$$\Pi(x_1, x_2) = \left( \frac{p_1x_1 + p_2x_2 + p_3}{p_7x_1 + p_8x_2 + 1}, \frac{p_4x_1 + p_5x_2 + p_6}{p_7x_1 + p_8x_2 + 1} \right)^T$$

It has eight degrees of freedom. These are determined by imposing the respective corners of the quadrilaterals which are mapped onto each other. The fingerprint is then the composition of all image information under the transformation of respective pairs of quadrilaterals from the traverse and the template grid. This defines a continuous piecewise projective transformation.

Unfortunately, this approach does not transfer smoothly into the 3D-case. Still in the 2D-case, this implies four appealing advantages. We are free to choose the sampling rate by proper choice of the template grid. As a by-product, we obtain a measurement for the blurring or distortion (Figs. 8i and 8j) with the absolute determinant of the Jacobian matrix of  $\Pi$ , which is defined in both the fingerprint domain and in  $\Omega$ . Furthermore, the mapping is invertible, so we can process the fingerprint and map any result back into the image geometry or even construct artificial cortex images with a given geometry (Fig. 6).

The quadrilateral grid of an ROI within the original data is presented in Figure 6a. In Figure 6b the rectangle  $Q_{k,l}$  is given by  $A, B, C, D$  and the projected rectangle  $R_{k,l}$  is given by  $A', B', C', D'$ . With fixed  $k$  and  $l$  whereas  $k \neq m, l \neq n$ , we define the four nodes  $A = Y^{k,l}$ ,  $B = Y^{k+1,l}$ ,  $C = Y^{k,l+1}$ ,  $D = Y^{k+1,l+1}$  on the grid. They are mapped to  $A', B', C'$  and  $D'$ , using the planar projective transformation  $\Pi$ . The transformed data in  $R_{k,l}$  are embedded in the cortical fingerprint (Fig. 6c).

### Quality Measurements and Parameters

The main measurement for the quality of the ED-, HY-, and HD-traverses is that they cross the neuronal

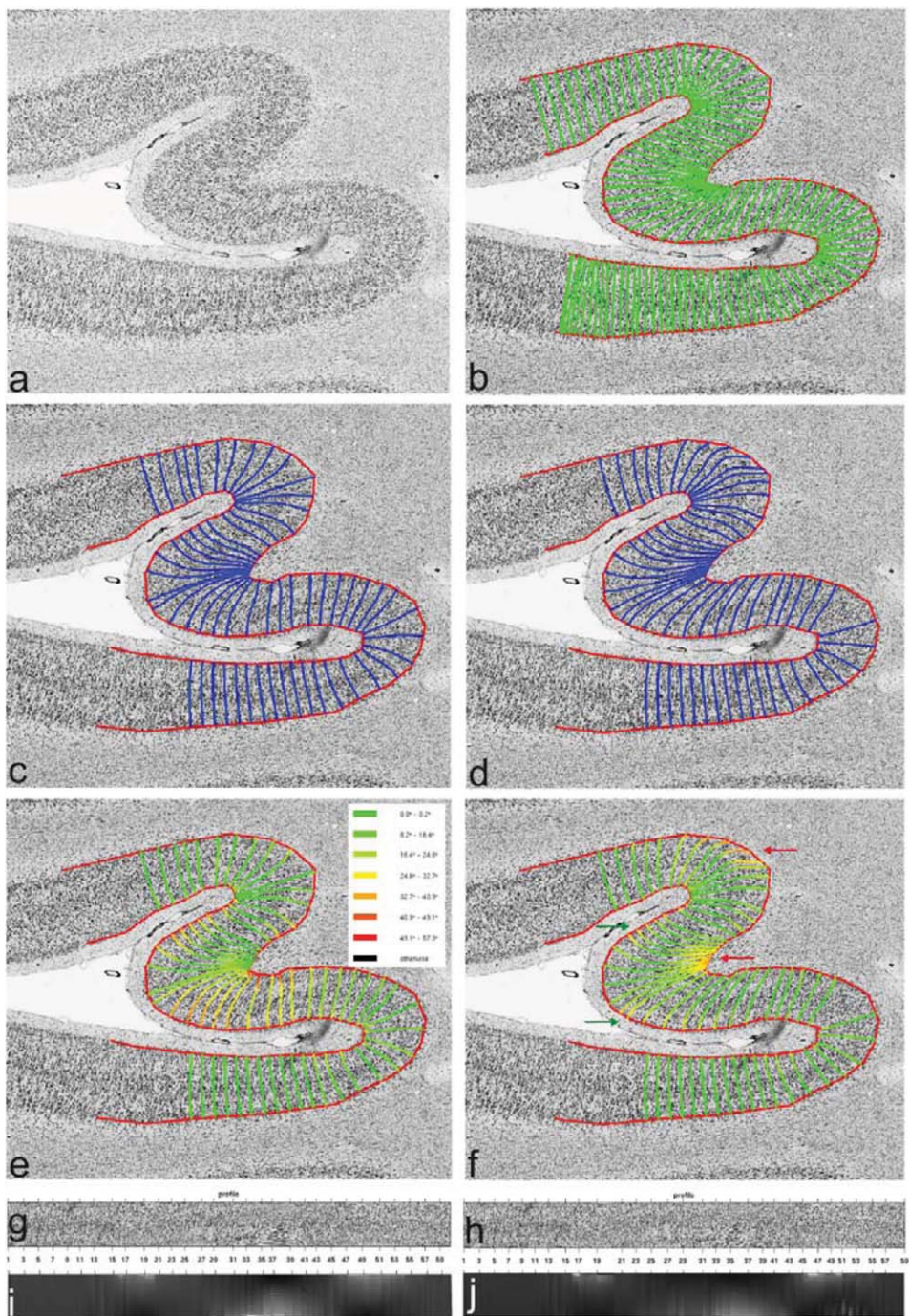


Fig. 8. **a:** The original image with a strongly curved part of the cerebral cortex. **b:** the ideal traverses (IT) in green. **c:** the EDT are shown in blue. **d:** the HT are shown in blue. **e:** The comparison of EDT and IT. Green encodes small and red large angular errors. The mean angular error is  $7.8^\circ$ . **f:** Comparison of IT and traverses computed by analyzing the electric field with local orientation. The mean absolute orientation difference is  $9.1^\circ$ . Green arrows indicate regions with stronger deviations from expected tra-

verses and red arrows point to regions where such strong deviations appear which are not found in the EDT. **g:** Fingerprint after affine projection of meshes based on EDT. **h:** Fingerprint after HY analysis where distortions (arrow) emerge. **i, j:** These correspond to (g, h) show the blurring derived from the determinant of the Jacobian of  $\Pi$  for all quadrilaterals. [Color figure can be viewed in the online issue, which is available at [wileyonlinelibrary.com](http://wileyonlinelibrary.com).]

layers of the cortex perpendicularly. As the layers cannot be extracted directly with any current computational method, we need to rely on manual input of ideal traverses. For simplicity, we define only straight line

traverses, which visually have the average ideal orientation. In this way, the visual improvement of the novel approach can be put into a figure, a kind of an average angular error  $\alpha$ . Let

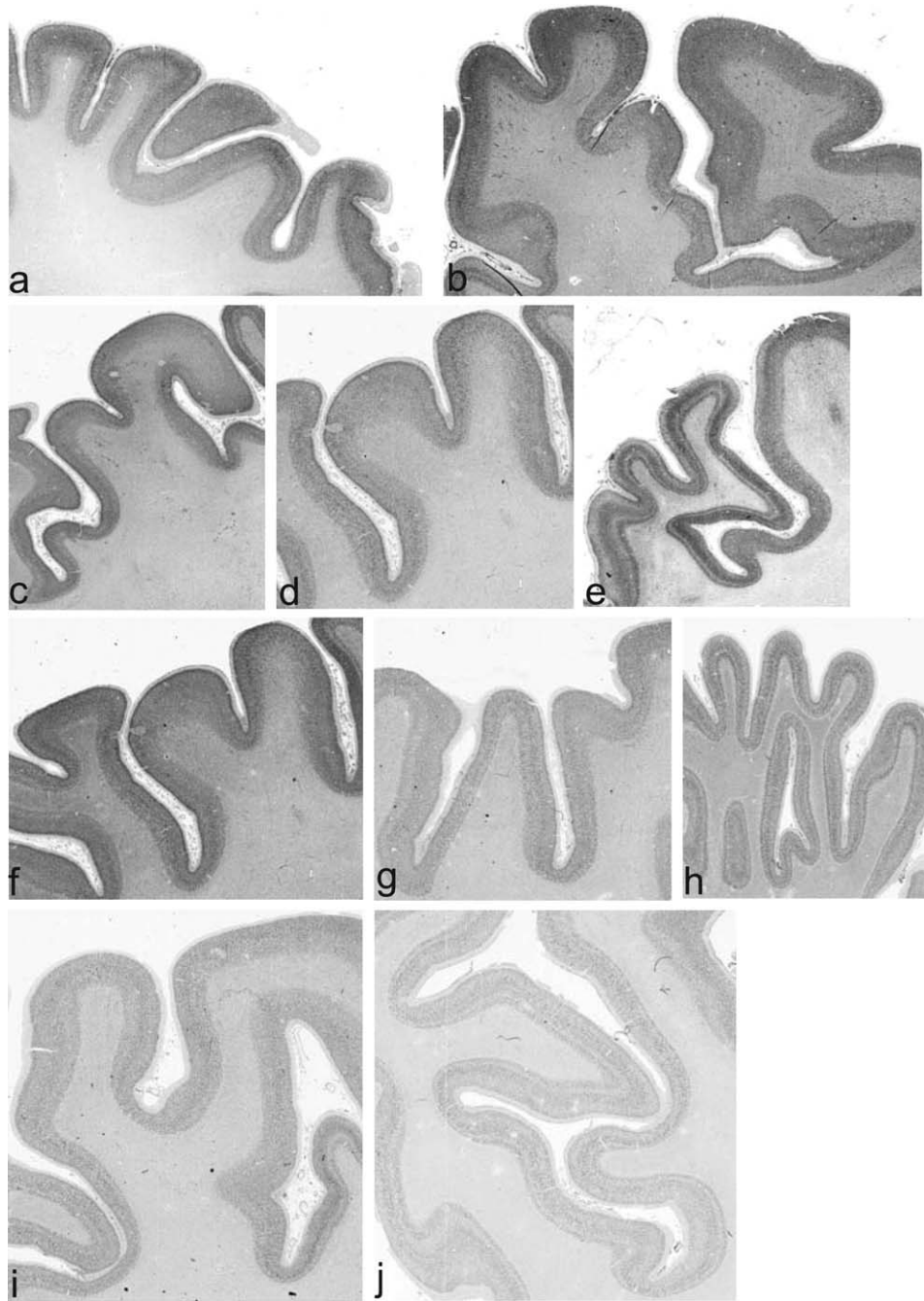


Fig. 9. Ten different regions of the cerebral cortex are used for statistical comparisons of the electrodynamic, hybrid, and hybrid-diffusion approaches.

$$Z^j = (Z^{j,l})_{l=0,1} \in H \times L, \quad j = 0, \dots, m'$$

$$Z^\kappa = (Z^{\kappa,l})_{l=0,1} \quad \kappa \in [0, m']$$

with

$$Z^{\kappa,l} = (\kappa - \lfloor \kappa \rfloor) Z^{[\kappa],l} + (1 - (\kappa - \lfloor \kappa \rfloor)) Z^{[\kappa]+1,l}$$

be the ideal traverse grid, and

$$Y_{l=0,\dots,n}^{k,l} \in \Omega^n, \quad k = 0, \dots, m$$

the computed traverse grid. We define an interpolation of the ideal traverse grid by

where  $\lfloor \cdot \rfloor$  denotes the greatest integer smaller than the number. The traverse-segment between the nodes  $Y_{k,l}^{k,l}$  and  $Y_{k,l+1}^{k,l+1}$  is judged by the angle  $\varphi_{k,l}$  that it encloses

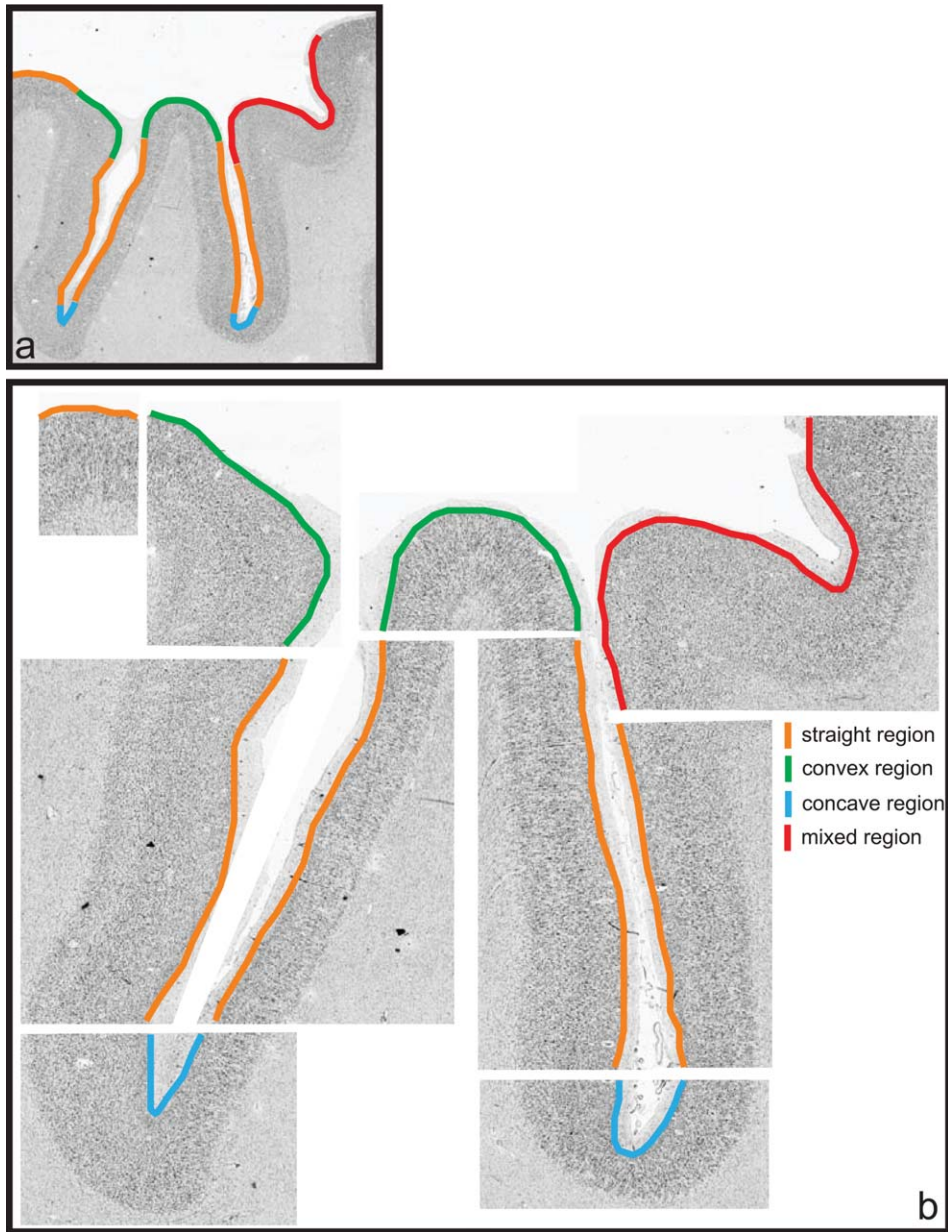


Fig. 10. Each sample region is subdivided and classified into straight, convex, concave, and regions with small convex and concave parts (mixed). Here, the same sample as in Figure 9g is used. **a:** The whole sample region is marked by different colors with respect to curvature classification as shown on the right in (b). **b:** The subdivision and classification of the whole sample region in sub sample images. [Color figure can be viewed in the online issue, which is available at [wileyonlinelibrary.com](http://wileyonlinelibrary.com).]

with  $Z^k$ , where  $\kappa$  is chosen so that the lines cross in  $(Y^{k,l} + Y^{k,l+1})/2$ .

Let  $E$  be the set and  $\#E$  the number of segments of traverses that can be judged this way. The angles  $\varphi$  between the ideal and the computed segments of traverses are averaged into the mean error measure  $\alpha$

$$\alpha := \frac{1}{\#E} \sum_{(k,l) \in E} \varphi_{k,l}$$

The HY-algorithm has several new parameters. The regularizer-variable  $\varepsilon$  is a small number, e.g.,  $10^{-4}$ . It should be small compared to 1 and well above the

arithmetic working-precision of the implementation. The integration-scale  $\rho$  of the structure tensor  $J$  (see section 3.2) can be chosen the same for the diffusion and the traverse generation. It should be the length of the neural columns in pixels (Sams and Agerkvist, 2002; Sams et al., 2004; Weickert, 1999). Therefore,  $\rho$  depends on the image resolution, and hence the methods are adaptable to this external parameter. For computing, we used a resolution of  $5 \mu\text{m}/\text{pixel}$  and a  $\rho$  of 64 pixels, which turns out to be appropriate.

The integration time  $T_2$  for the coherence-enhancing diffusion should be great enough so that the result is nearly constant in time.

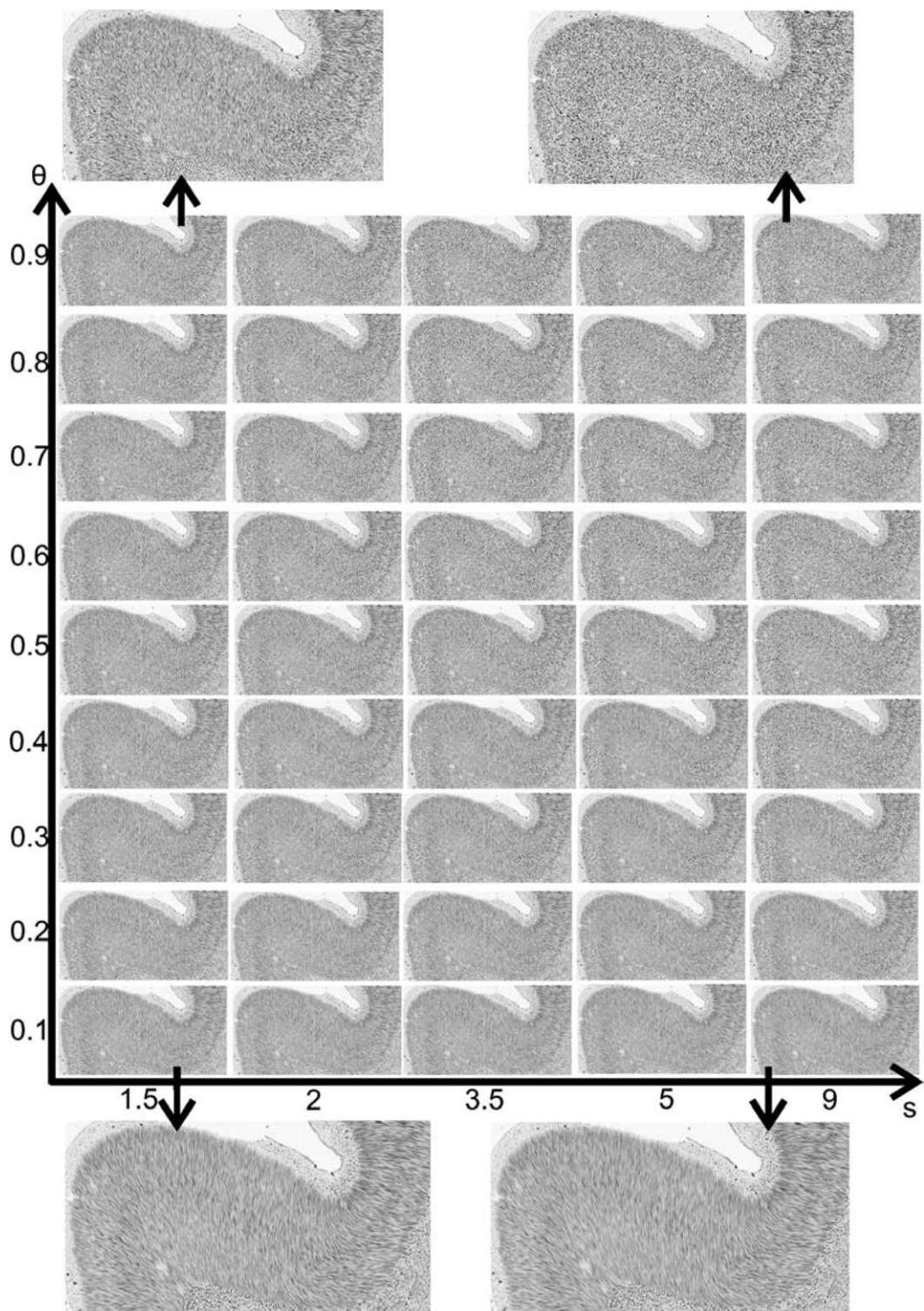


Fig. 11. To determine and compare optimal diffusion parameters for minimizing  $\alpha$  the parameters  $\theta$  and  $s$  are adapted to each of the 10 sample images. The resulting diffusion images are sub sampled according to the scheme shown in Figure 10. The subregion in the upper right corner of Figure 10 is classified as mixed.

This image is used here to present the effects of diffusion by parameter variation of  $\theta$  and  $s$ . The four larger images belong to the smaller images of the sample matrix. The strongest diffusion can be seen for  $\theta = 0.1$  and  $s = 1.5$ . The lowest diffusion image is calculated with  $\theta = 0.9$  and  $s = 9$ .

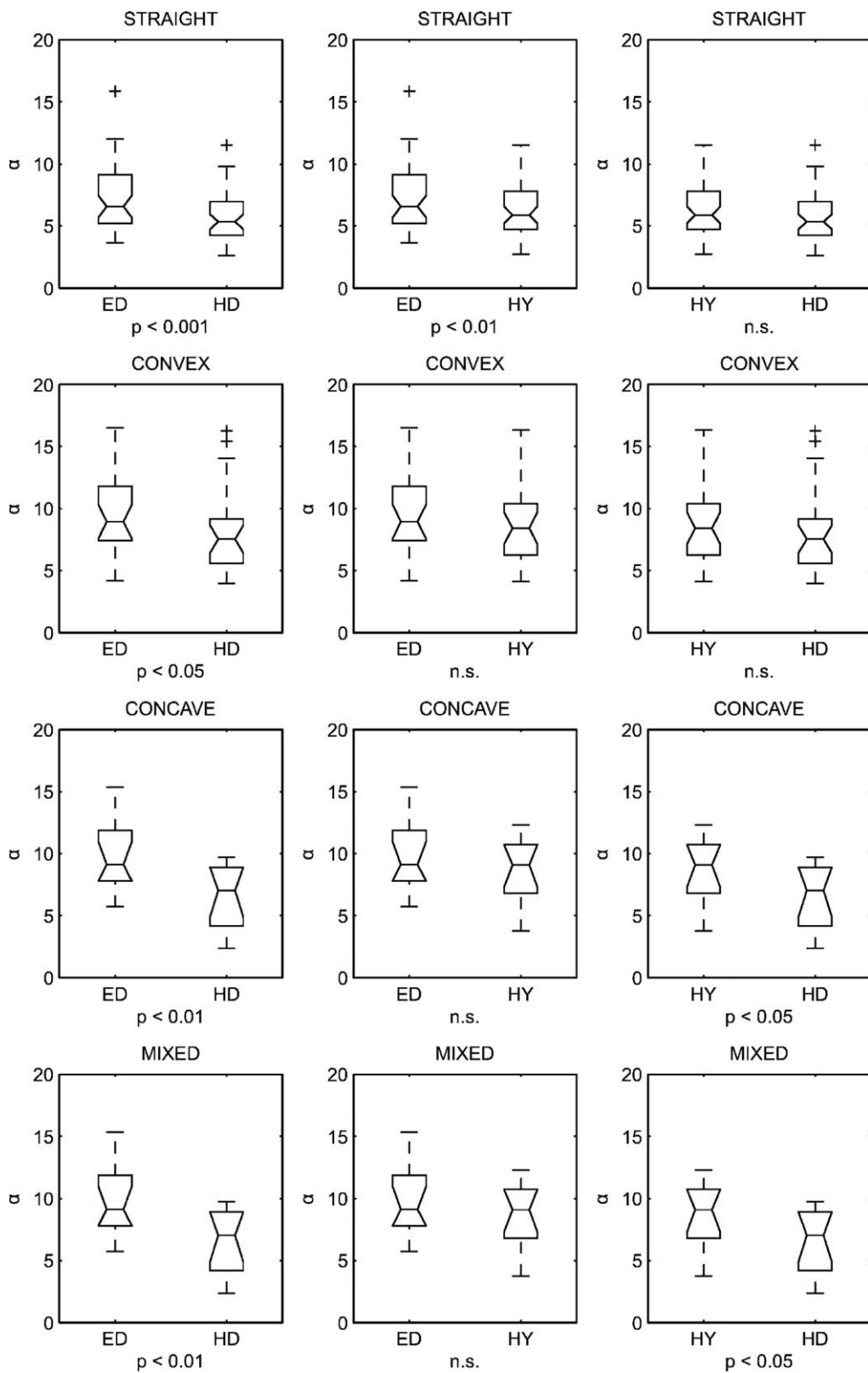


Fig. 12. Null hypotheses are tested for ED, HY, and HD. A significant ( $p \leq 0.05$ ) smaller  $\alpha$  is found by HD with regard to HY and ED within straight, concave, and mixed subregions. HY generates smaller values of  $\alpha$  with respect to ED within straight and mixed subregions.

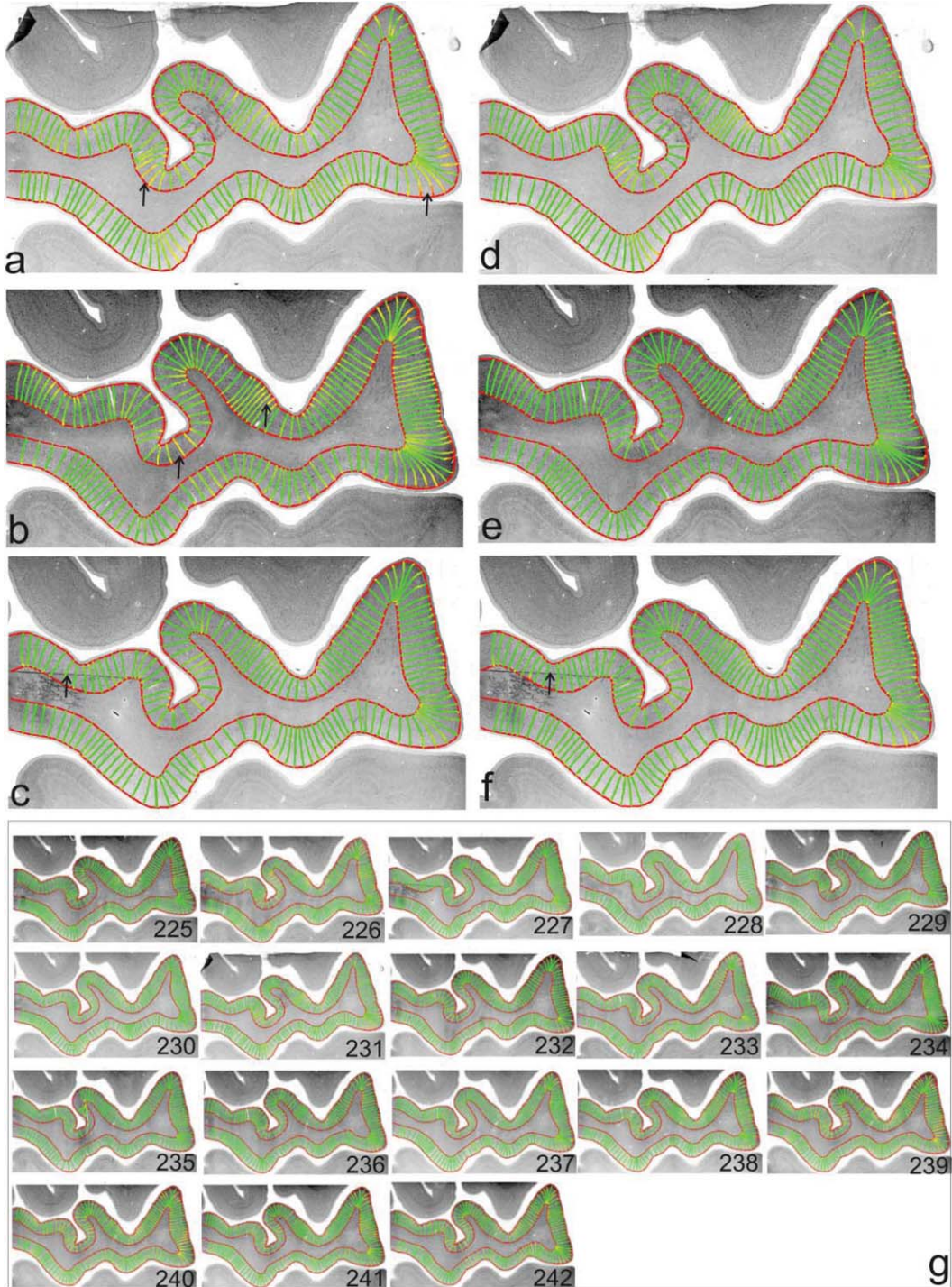


Fig. 13. The ED and HY results of an analysis of a contiguous stack of histological images. **a, b:** Two examples of ED traverses. The local error  $\varphi$  (see section 3.6) is color coded. The arrows are pointing to regions with strong deviations from ideal traverses. **c:** An artifact (arrow) does not disturb the generation of traverses by ED. **e, f:** The same sections as shown in (b) and (c). Traverses

are computed with the HD method, no such strong deviations as generated by ED can be seen here. **f:** The artifact does not have a stronger influence on the traverses passing it. **g:** Overview of all scanned sections of this stack analysis using the HD method. [Color figure can be viewed in the online issue, which is available at [wileyonlinelibrary.com](http://wileyonlinelibrary.com).]

The grid-parameters  $m, n, (t_l)_{l=1}^n$  can be chosen so that the grid becomes uniform and the meshes  $Q^{k,l}$  enclose nearly the same surface area. The choice of the starting points  $y_0^k$  is done in a specific recursive way.

The remaining parameters are  $s$  and  $\theta$  for the probability of local existence of neural columns  $\beta$ . Their choice, different for diffusion and traverse generation, strongly depends on the image data because they

control which structural feature is assumed to be a neural column and which is not. We optimized these parameters for different image samples with respect to  $\alpha$  and derived rules for the provided data-sets containing the ideal traverses, contours, and ROIs. Remarkably,  $\lim_{\theta \rightarrow 1} \beta = 0$ . This means that the ED is a special case of HY. This results in the fact that HY and HD with optimal parameters can at least not get worse than ED. Still, it would be important to obtain hints about the existence of global optimal parameters.

Figure 7 clearly shows that the distributions of angles  $\varphi$  (mean angular difference of computed traverses with regard to ITs) for the ED and the HD are different. The ED leads to fewer small and more large angular errors with regard to HD where many small  $\varphi$  and less large  $\varphi$  are computed. This means that the HD computes traverses, which are more similar with the IT than the ETs.

## RESULTS

The traverses calculated by the ED, HY, and HD approaches are compared with traverses defined by a person experienced in cytoarchitectonic analysis. The expert-defined traverses are called ideal traverses (IT). The IT are defined over the whole inner and outer contour of a cortical sample image (Fig. 9). The local deviation of the traverses calculated by ED to the ideal traverses is shown in Figure 8. The evaluation is done in terms of the relative comparison of the deviation of mean angles  $\alpha$  of ED traverses and ideal traverses.

### Visualization

The local deviation of angles has been color coded to visualize local differences of traverse orientation (see inset in Fig. 8e). There are two regions of the cortex shown in Figure 8, where the advantage of the hybrid method can be recognized. These are the small straight segments before and after the central convex part in this example. The orientation of cells in these subregions is not orthogonal to the inner and outer surface; rather, they have an oblique orientation. The traverses of the hybrid technique follow these local oblique orientations of cells. This can be verified by relatively small traverse deviations of IT and hybrid traverses (HT). Furthermore, blurring effects introduced by sampling the gray values between neighboring traverses are smaller for the hybrid technique than for the electrodynamic approach, cf. Figures 8g–8h.

To find out if this preliminary observation turns out to be consistent within different cortex samples with strong changes of curvature and local orientation of cells, a statistical analysis was performed. Ten different samples of larger regions of cortex were used in Figure 9. Ideal traverses were defined for those parts of the cerebral cortex that can be continuously outlined. Subregions were classified by the local curvature into straight, convex, concave, and mixed parts (Fig. 10). Within each subregion, the values  $\alpha$  of the ED and HY methods are determined. A diffusion scheme is solved for all ten cortex samples followed by a HD traverse calculation and IT comparison. The intensity of diffusion is controlled by two parameters. Therefore, 45 combinations of these parameters produce 45 different diffusion weighted images (Fig. 11). From each of these diffusion weighted sample images, the same

subimages are cropped as for the ED and HY evaluation. The diffusion preprocessed subimages are explored by the same variations of  $\theta$  and  $s$  as within the HD approach.

### Quality Measurement $\alpha$

To evaluate the outcome of the methods ED, HD, and HY, we applied the algorithms to obvious complex and large cortical regions normally not found in figures of the cortical mapping literature. Furthermore, we tested the algorithms ED and HY on a serially sectioned region of area 6 (Fig. 13).

The mean values of  $\alpha$  and S.E.M.s within the straight samples are  $7.3^\circ \pm 0.36^\circ$  (ED),  $6.3^\circ \pm 0.29^\circ$  (HY), and  $5.7^\circ \pm 0.28^\circ$  (HD). For the convex samples, the HD methods turns out to generate the smallest  $\alpha$  of  $8.34^\circ \pm 0.74^\circ$  whereby as HY produces a mean  $\alpha$  of  $10.1^\circ \pm 0.82^\circ$  and ED a mean  $\alpha$  of  $9.0^\circ \pm 0.77^\circ$ . When testing the concave regions, a mean  $\alpha$  of  $6.7^\circ \pm 0.67^\circ$  for HD, a mean  $\alpha$  of  $8.4^\circ \pm 0.66^\circ$  for HY, and the largest mean  $\alpha$  of  $9.8^\circ \pm 0.75^\circ$  was found for ED. The more complex mixed regions consisting of smaller convex and concave or straight parts show larger mean  $\alpha$ s than the previous types of cortex curvatures. Just as in the other results, the HD shows a smallest mean  $\alpha$  of  $9.3^\circ \pm 1.12^\circ$ , the HY a mean  $\alpha$  of  $11.3^\circ \pm 1.43^\circ$ , and the ED a mean  $\alpha$  of  $13.5^\circ \pm 1.77^\circ$ .

The serially sectioned area 6 of the human cerebral cortex showed a strong correlation of local  $\alpha$ s from section to section.  $\alpha$  was significantly smaller in comparison to the ED evaluation. Even if there occur artifacts no disturbances of the traverse paths can be observed. Therefore, it can be concluded that HY is robust with regard to artifacts and produce similar results if local orientation information of adjacent serial sections is correlated.

### Statistics

The mean  $\alpha$  for the straight, convex, concave, and mixed samples are compared with regard to significance ( $p \leq 0.05$ ) by the two-tailed Mann-Whitney-U-test because the distributions are not normal (Fig. 12). The hybrid method has a significantly smaller deviation of  $\alpha$  than the electrodynamic method (Fig. 12) when applied to straight courses of cortex. An additional diffusion preprocess in combination with the hybrid method turns out to be significant for all types of cortical courses, i.e., straight, convex, concave, and mixed (Fig. 12). However, at a level of  $p \leq 0.01$  convex regions are not significant. Interestingly, significantly smaller deviations of  $\alpha$  are found for the HD method in comparison with the HY method with regard to concave and mixed courses of the cerebral cortex sub samples (Fig. 12). Structural changes of cytoarchitecture are more likely to occur between sections farther away than between adjacent sections. Hence, differences of  $\alpha$  in cytoarchitecturally similar or adjacent sections should be small, too. We prove that structurally related parts of neighboring sections of a stack of consecutive sections (tissue volume) lead to significant differences of  $\alpha$ . In a comparison of  $\alpha$ s in the second example of adjacent histological sections of area 6, no significant differences were found (Fig. 13).

### Optimal Parameters

Based on the statistical comparisons, the HD approach shows the smallest  $\alpha$ . By investigating the parameter space for controlling the coherence and the diffusion, we found that parameters converge to similar values for the four basic cortex curvatures. Optimal diffusion parameters are  $\theta = 0.7$  and  $s = 5.8$ . For the hybrid part (HY) an optimal hybrid  $\theta$  of 0.41 and a hybrid  $s$  of 7.5 is determined.

### DISCUSSION

The idea of orthogonal scanning of the cerebral cortex was first published by Hopf (1966) and Hudspeth et al., (1976); whereas earlier attempts of quantitative analysis had been made by von Economo et al. (2007) and Bok (1959). This way of quantifying cytoarchitectonics has been developed and investigated especially by Schleicher et al. (Schleicher and Zilles, 1990; Schleicher et al., 1978, 1986, 1998, 1999, 2000, 2005). The method of calculating traverses has been refined by an electrodynamic model with curved capacitor plates allowing traverses to follow isoelectric paths (Schmitt and Böhme, 2002). Principally, orthogonal scanning is the first step of sampling cytoarchitectonic data of the cerebral cortex for subsequent statistical analysis (Schleicher et al., 2000, 2005; Schmitt et al., 2003). Furthermore, observer-independent cytoarchitectonic parcellation of the cerebral cortex is the foundation for the development of a reliable digital cytoarchitectonic atlas. Such an atlas is still under construction (Amunts and Zilles, 2001; Amunts et al., 1998, 1999a,b, 2000b; Geyer et al., 1996, 1997, 1999, 2000; Zilles and Palomero-Gallagher, 2001; Zilles et al., 1995, 1996, 2004) because of the highly complex and painstaking analytic work. This cytoarchitectonic atlas, containing a revised and improved Brodmann areal labeling scheme, provides the best known source for relating activated regions in fMRI to cytoarchitectonic areas (Devlin and Poldrack, 2007). It is mandatory to optimize the method that generates the scanning of cytoarchitecture to analyze a data structure containing minimal distortions with regard to local lamination orientation introduced by the scanning method.

To obtain a data structure (profile) by scanning that reflects an almost nonblurred progression of the cytoarchitecture, the sampling should be locally orthogonal to the underlying cell distribution constituting the cortical lamination. This is partially fulfilled by approximation when using information of the cortical surface and of the white matter border only. Beside the basic information of the inner and outer border of the cerebral cortex, most information is contained in the local distribution of cells. The local distribution of cells can be stochastically considered as complex multimodal cluster processes always running more or less parallel to the inner and outer surfaces intermingled not in each area by cytoarchitectonic cell columns (minicolumns) or vertical cell clusters oriented approximately perpendicular to the cytoarchitectonic lamination (Buxhoeveden et al., 2000; Casanova et al., 2007; Mountcastle, 1997; Rockland and Ichinohe, 2004). However, the local orientation of cell columns may not be suitable in each histological section because columns may not occur in a specific region or the orienta-

tion of sectioning is tangential to the lamination parallel to, e.g., layer 2 and columns are not or only partially visible.

To overcome the latter problem, we combine two approaches: the basic electrodynamic model and local orientation of cells (Rao and Schunck, 1991). This approach guarantees reliable generation of traverses in those regions containing insufficient local orientation measured by the coherence. Therefore, the hybrid approach can be used either in cortical regions where strong cell columns occur and in those where they are absent or not suitable due to sectioning. Increase of the resolution of angles of the gradient operator  $\nabla f_\sigma$  may provide further accuracy, however, this needs to be investigated with regard to the relation of given resolution and accuracy increase. The local orientation the coherence can be enhanced by anisotropic diffusion filtering (Black et al., 1998; Perona, 1998; Perona and Malik, 1990; Weickert, 1997, 1998) on cortical cytoarchitectonics. The anisotropic diffusion filter must be restricted to the cerebral cortex. Otherwise, local orientation of the white matter or suprapial space may disturb the local orientation patterns in the ROI. This concept of local restricted anisotropic diffusion filtering is first published here.

Beside anisotropic Gauss filtering in orientation scale space (Geusebroek et al., 2003), a further promising approach is the combination of evaluating local orientation by principal component analysis (PCA) and multiscale pyramid decomposition (MPD) (Feng and Milanfar, 2002) to find the maximum likelihood estimate of local orientation. PCA and MPD turn out to produce smooth orientation fields, if data are corrupted by noise. As the lamination of the cerebral cortex is a curved oriented pattern represented by a microtexture of single cells, curvilinear models may turn out to be suitable. These models estimate local curvature by means of parabolic and circular structures and may yield quantitative access to tangential curvatures (van de Weijer et al., 2001) typical for the cortical ribbon.

In the past, sampling is done simply by calculating testlines and extracting gray values covered by the testline. Therefore, many testlines need to be calculated to obtain an appropriate profile for statistical analysis. Here, we apply the concept of projective transformation where an area around a local testline is transformed to the profile. This procedure reduces the sampling time; however, more importantly, the blurring effect is diminished. In the past, sampling is achieved by calculating neighboring testlines. As a new approach we propose a recursive subdivision of the ROI in combination with a projective piecewise transformation.

The electrodynamic model, the hybrid method, and the hybrid diffusion method are compared statistically. For this purpose, ideal traverses are defined in cortical ROIs of 10 different parts of the cerebral cortex containing strong curvature changes and varying degrees of cell columns. Furthermore, subregions were defined in the 10 basic sample images. The subregions are classified into four types of curvature: straight, convex, concave, and mixed cortical courses. We find significantly lower  $\alpha$  deviations of the hybrid diffusion method with regard to the electrodynamic approach. In a second example, we have determined  $\alpha$ s of serial sections and found no significant differences of  $\alpha$ s.

Therefore, we provide evidence for the better (smaller  $\alpha_s$  by algorithm comparison) and robust (no significant differences of  $\alpha_s$  of adjacent sections with similar cytoarchitectonics and curvature of the brain surface) hybrid diffusion method.

A complementary procedure for quality control could be the definition of layer borders and the comparison of testlines orthogonal to the defined layer borders with the computed traverses.

Finally, the parameter space is investigated. Interestingly, independent of the type of curvature, the optimal parameters of the diffusion enhancement and of the function  $\beta$  lie in similar ranges. However, further investigations may answer the question if these parameters should be refined and optimized in dependence of the local curvature and local curvature scale space (Cao, 2003).

Image registration techniques allow to analyze cytoarchitecture at high resolution in 3D (Modersitzki, 2004; Schmitt et al., 2005, 2007, 2008). Therefore, an important development of the current intuitive approach of considering the orientation of cell distributions to guide nonlinear traverses is its extension to 3D. In particular, the local orientation and the restricted anisotropic diffusion need to be extended. Because the computational complexity increases paralleling the computation of the techniques of anisotropic diffusion, local orientation and the electrodynamic model will be inevitable.

Different patterns of staining are clearly visible by comparing the sample images in Figure 9. Therefore, further improvements may be possible by choosing an advanced prepossessing scheme with regard to homogenization of texture measures like contrast of the cooccurrence matrix of histological cortex images. Such normalizations need to be investigated systematically to reduce variability of  $\theta$  and  $s$  for the local orientation coherence.

More complex work is waiting concerning the definition of contours and automatic outlining of layers. The realization of automatic surface parallel outlining methods may provide more reliable data supporting the computing of local optimal paths for cytoarchitectonic scanning.

Using ODEs is the least invasive approach to introduce the image information into the electrodynamic model. The latter could be extended to a PDE model (Annese et al., 2004; Jones et al., 2000). A traverse could be computed as a falling line of a potential, which is the solution of a boundary-value problem of a PDE. Image anisotropy could be introduced with the structure-tensor much like in the coherence-enhancing diffusion model. The computational burden is hard to assess, but severe code-optimization will not be avoidable in such a model. The burden on the computational side would ease the technical difficulties on the theoretical side. Alongside a beautiful theory, there might be room for a hybrid model with less and more meaningful parameters, which might be better adaptable to the data. Furthermore, the 3D case could be derived more smoothly. This research, however, is out of the scope of this paper.

The curvilinear paths of traverses are often reminiscent of migration paths and morphology of migrating radial glia (Rakic, 2003) (reverse path finding) and,

therefore, seem to match rather precisely the internal geometry of the cerebral cortex. This observation may be verified by radial glia staining and a stepwise development dependent comparison of cortical path distributions.

In conclusion, we have developed a new hybrid method following the intuitive visually recognizable cortex borders in combination with local cell distributions by methods of computer vision (anisotropic diffusion, local orientation), physical modeling (electrodynamic), and mapping (projective transformation) techniques. It is shown that the new anisotropic diffusion enhanced hybrid approach has a statistically significant smaller deviation to expert-defined ideal traverses in different types of curvature in comparison to the electrodynamic or hybrid method without diffusion enhancement.

## ACKNOWLEDGMENTS

The authors thank Manfred Tasche of the Institute for Mathematics of the University of Rostock for sharing his expertise and superior help in preparing the manuscript. They appreciate Andreas Wree of the Department of Anatomy for his critical discussions on cytoarchitectonics. They thank Martin Böhme (Institute for Neuro- and Bioinformatics, University of Lübeck) for his constructive contributions of realizing the electric field model and discussion of the new hybrid approach. Especially, they would like to thank Karl Zilles and Katrin Amunts for making the histological brain sections of outstanding quality available for this study.

## REFERENCES

- Amunts K, Zilles K. 2001. Advances in cytoarchitectonic mapping of the human cerebral cortex. *Neuroimaging Clin North Am* 11:151–169.
- Amunts K, Klingberg T, Binkofski F, Schormann T, Seitz R, Roland P, Zilles K. 1998. Location, asymmetry and variability of human areas 17 and 18. *NeuroImage* 7:8.
- Amunts K, Schleicher A, Bürgel U, Mohlberg H, Uylings H, Zilles K. 1999a. Broca's region revisited: Cytoarchitecture and intersubject variability. *J Comp Neurol* 412:319–341.
- Amunts K, Schormann T, Mohlberg H, Malikovic A, Zilles K. 1999b. Location, asymmetry and variability of human areas 17 and 18. *NeuroImage* 9:861.
- Amunts K, Jancke L, Mohlberg H, Steinmetz H, Zilles K. 2000a. Interhemispheric asymmetry of the human motor cortex related to handedness and gender. *Neuropsychologia* 38:304–312.
- Amunts K, Malikovic A, Mohlberg H, Schormann T, Zilles K. 2000b. Brodmann's areas 17 and 18 brought into stereotaxic space—where and how variable? *NeuroImage* 11:66–84.
- Annese J, Pitiot A, Dinov I, Toga A. 2004. A myelo-architectonic method for the structural classification of cortical areas. *NeuroImage* 21:15–26.
- Bailey P, von Bonin G. 1951. The isocortex of man. Urbana: University of Illinois Press.
- Bartels A, Zeki S. 2005. The chronoarchitecture of the cerebral cortex. *Phil Trans R Soc B* 360:733–750.
- Bigün J, Granlund G. 1987. Optimal orientation detection of linear symmetry. *Proc ICCV*, 1:433–438.
- Black M, Sapiro G, Marimont D, Heeger D. 1998. Robust anisotropic diffusion. *IEEE Trans Imag Proc* 7:421–432.
- Bok S. 1959. *Histology of the cerebral cortex*. Amsterdam: Elsevier Publishing Company.
- Borostyankoi-Baldauf Z, Herczeg L. 2002. Parcellation of the human pretectal complex: a chemoarchitectonic reappraisal. *Neuroscience* 110:527–540.
- Braak H. 1980. *Architectonics of the human telencephalic cortex. Studies of brain function*. Berlin: Springer.
- Brodmann K. 1909. *Vergleichende Lokalisationslehre der Grosshirnrinde in ihren Prinzipien dargestellt auf Grund des Zellenbaues*. Leipzig: Barth.

- Buxhoeveden D, Casanova M. 2002. Quantitative analysis of cell columns in the cerebral cortex. *Brain* 125:935–951.
- Buxhoeveden D, Switala A, Roy E, Casanova M. 2000. Quantitative analysis of cell columns in the cerebral cortex. *J Neurosci Methods* 97:7–17.
- Campbell A. 1905. Histological studies on the localization of cerebral function. Cambridge: University Press.
- Cao F. 2003. Geometric curve evolution and image processing. LNM 1805:1–187.
- Casanova M, Trippe J, Switala A. 2007. A temporal continuity to the vertical organization of the human neocortex. *Cereb Cortex* 17:130–137.
- Chambers D, Fishell G. 2006. Functional genomics of early cortex patterning. *Genome Biol* 7:1–4.
- Choi H-J, Zilles K, Mohlberg H, Schleicher A, Fink G, Armstrong E, Amunts K. 2006. Cytoarchitectonic identification and probabilistic mapping of two distinct areas within the anterior ventral bank of the human intraparietal sulcus. *J Comp Neurol* 495:53–68.
- Devlin J, Poldrack R. 2007. In praise of tedious anatomy. *NeuroImage* 37:1033–1041.
- De Vos K. 1999. Personal communication. Netherlands Institute of Brain Research, Amsterdam.
- Eickhoff S, Walters N, Schleicher A, Kril J, Egan G, Zilles K, Watson J, Amunts K. 2005. High-resolution MRI reflects myeloarchitecture and cytoarchitecture of human cerebral cortex. *Hum Brain Mapp* 24:206–215.
- Elliot Smith G. 1907. A new topographical survey of the human cerebral cortex, being an account of the anatomically distinct cortical areas and their relationship to the cerebral sulci. *J Anat* 41:237–254.
- Feng X, Milanfar P. 2002. Multiscale principal components analysis for image local orientation estimation. *Signals, Systems and Computers*, 2002. Conf Rec Thirty-Sixth Asilomar Conf 1:478–482.
- Feng Y, Olson E, Stukenberg P, Flanagan L, Kirschner M, Walsh C. 2000. LIS1 regulates CNS Lamination by interacting with mNudE, a central component of the centrosome. *Neuron* 28:665–679.
- Filimonoff I. 1932. Über die Variabilität der Großhirnrindenstruktur. Mitteilung II - Regio occipitalis beim erwachsenen Menschen. *J Psychol Neurol* 44:2–96.
- Geusebroek JM, Smeulders AWM, van de Weijer J. 2003. Fast anisotropic gauss filtering. *IEEE Trans Image Process* 12 (8):938–943.
- Geyer S, Ledberg A, Schleicher A, Kinomura S, Schormann T, Buerger U, Klingberg T, Larsson J, Zilles K, Roland P. 1996. Two different areas within the primary motor cortex of man. *Nature* 382:805–807.
- Geyer S, Schleicher A, Zilles K. 1997. The somatosensory cortex of human: cytoarchitecture and regional distributions of receptor-binding sites. *NeuroImage* 6:27–45.
- Geyer S, Schleicher A, Zilles K. 1999. Areas 3a, 3b, and 1 of human primary somatosensory cortex. I. Microstructural organization and interindividual variability. *Neuroimage* 10:63–83.
- Geyer S, Schormann T, Mohlberg H, Zilles K. 2000. Areas 3a, 3b and 1 of human somatosensory cortex. II. Spatial normalization to standard anatomical space. *Neuroimage* 11:684–696.
- Granlund G, Knutson H. 1995. Signal processing for computer vision. Dordrecht: Kluwer Academic Publishers.
- Hevner R, Daza R, Rubenstein J, Stunnenberg H, Olavarria J, Englund C. 2003. Beyond laminar fate: Toward a molecular classification of cortical projection/pyramidal neurons. *Dev Neurosci* 25:139–151.
- Hofp A. 1966. Über eine Methode zur objektiven Registrierung der Myeloarchitektonik der Hirnrinde. *J Hirnforsch* 8:302–313.
- Hofp A. 1968a. Photometric studies on the myeloarchitecture of the human temporal lobe. *J Hirnforsch* 10:285–297.
- Hofp A. 1968b. Registration of the myeloarchitecture of the human frontal lobe with an extinction method. *J Hirnforsch* 10:259–269.
- Horton J, Adams D. 2005. The cortical column: A structure without a function. *Phil Trans R Soc B* 360:837–862.
- Hudspeth A, Ruark J, Kelly J. 1976. Cytoarchitectonic mapping by microdensitometry. *Proc Natl Acad Sci USA* 73:2928–2931.
- Huettel S, Song A, McCarthy G. 2004. Functional magnetic resonance imaging. Sunderland: Sinauer Associates.
- Jacobowitz D, Kresse A, Skofitsch G. 2004. Galanin in the brain: chemoarchitectonics and brain cartography—A historical review. *Peptides* 25:433–464.
- Jähne B. 2004. Practical handbook on image processing for scientific and technical applications. Boca Raton: CRC Press.
- Jones S, Buchbinder B, Aharon I. 2000. Three-dimensional mapping of cortical thickness using laplace's equation. *Hum Brain Mapp* 11:12–32.
- Lashley K, Clark G. 1946. The cytoarchitecture of the cerebral cortex of atelots: A critical examination of architectonic studies. *J Comp Neurol* 85:223–305.
- Mallamaci A, Stoykova A. 2006. Gene networks controlling early cerebral cortex arealization. *Eur J Neurosci* 23:847–856.
- Mazziotta J, Toga A, Evans A, Fox P, Lancaster J, Zilles K, Woods R, Paus T, Simpson G, Pike B, Holmes C, Collins L, Thompson P, Macdonald D, Iacoboni M, Schormann T, Amunts K, Palomero-Gallagher N, Geyer S, Parsons L, Narr K, Kabani N, Goualher GL, Feidler J, Smith K, Boomsma D, Pol HH, Cannon T, Kawashima R, Mazoyer B. 2001. A four-dimensional probabilistic atlas of the human brain. *J Am Med Inf Assoc* 8:401–430.
- Merker B. 1983. Silver staining of cell bodies by means of physical development. *J Neurosci Methods* 9:235–241.
- Mitrofanis J, Ashkan K, Wallace B, Benabid A. 2004. Chemoarchitectonic heterogeneities in the primate zona incerta: Clinical and functional implications. *J Neurocytol* 33:429–440.
- Modersitzki J. 2004. Numerical methods for image registration. Oxford University Press, New York.
- Mountcastle V. 1997. The columnar organization of the neocortex. *Brain* 120:701–722.
- Perona P. 1998. Orientation diffusions. *IEEE Trans Image Process* 7 (3):457–467.
- Perona P, Malik J. 1990. Scale space and edge detection using anisotropic diffusion. *Pat Anal Mach Intel* 12:629–639.
- Pfeifer R. 1940. Die angioarchitektonische areale Gliederung der Grosshirnrinde. Barth: Leipzig.
- Rakic P. 1988. Specifications of cerebral cortical areas. *Science* 241:170–176.
- Rakic P. 2003. Developmental and evolutionary adaptions of cortical radial glia. *Cereb Cortex* 13:541–549.
- Rao A, Schunck B. 1991. Computing oriented texture fields. *CVGIP: Graph Models Image Process* 53 (2):157–185.
- Rockland K, Ichinohe N. 2004. Recursive segmentation of minicolumns using myelinated bundles. *Exp Brain Res* 158:265–277.
- Roland P, Geyer S, Amunts K, Schormann T, Schleicher A, Malikovic A, Zilles K. 1997. Cytoarchitectural maps of the human brain in standard anatomical space. *Hum Brain Mapp* 5:222–227.
- Roland P, Zilles K. 1998. Structural divisions and functional fields in the human cerebral cortex. *Brain Res Rev* 26:87–105.
- Rosano C, Sweeney J, Melchitzky D, Lewis D. 2003. The human precentral sulcus: Chemoarchitecture of a region corresponding to the frontal eye fields. *Brain Res* 972:16–30.
- Sams T, Agerkvist F. 2002. Coherence enhancing diffusion filtering of sidescan sonar images. Tech. rep., Danish Defence Research Establishment, DDRE report F-38/2002, Copenhagen, Denmark.
- Sams T, Hansen J, Thisen E, Stage B. 2004. Segmentation of sidescan sonar images. Tech. rep., Danish Defence Research Establishment, DDRE report M-21/2004, Copenhagen, Denmark.
- Schleicher A, Zilles K. 1990. A quantitative approach to cytoarchitectonics: analysis of structural inhomogeneities in nervous tissue using an image analyser. *J Microsc* 157:367–381.
- Schleicher A, Zilles K, Kretschmann H-J. 1978. Automatische Registrierung und Auswertung eines Grauwertindex in histologischen Schnitten. *Verh Anat Ges* 72:413–415.
- Schleicher A, Ritzdorf H, Zilles K. 1986. A quantitative approach to cytoarchitectonics: Software and hardware aspects of a system for the evaluation and analysis of structural inhomogeneities in nervous tissue. *J Neurosci Methods* 18:221–235.
- Schleicher A, Amunts K, Geyer S, Kowalski T, Zilles K. 1998. Observer-independent cytoarchitectonic mapping of the human cortex using a stereological approach. *Acta Stereol* 17:75–82.
- Schleicher A, Amunts K, Geyer S, Morosan P, Zilles K. 1999. Observer-independent method for microstructural parcellation of cerebral cortex: a quantitative approach to cytoarchitectonics. *Neuroimage* 9:165–177.
- Schleicher A, Amunts K, Geyer S, Kowalski T, Schormann T, Palomero-Gallagher N, Zilles K. 2000. A stereological approach to human cortical architecture: Identification and delineation of cortical areas. *J Chem Neuroanat* 20:31–47.
- Schleicher A, Palomero-Gallagher N, Morosan P, Eickhoff S, Kowalski T, de Vos K, Amunts K, Zilles K. 2005. Quantitative architectural analysis: A new approach cortical mapping. *Anat Embryol* 210:373–386.
- Schmitt O, Böhme M. 2002. A robust transcranial profile scanner for generating 2D-traverses in histological sections of rich curved cortical courses. *NeuroImage* 16:1103–1119.
- Schmitt O, Hörmke L, Dümbgen L. 2003. Detection of cortical transition regions utilizing statistical analyses of excess masses. *NeuroImage* 19:42–63.
- Schmitt O, Pakura M, Aach T, Böhme M, Bock S, Preuse S. 2004. Analysis of nerve fibers and their distribution in histologic sections of the human brain. *Micr Res Tech* 63:220–243.

- Schmitt O, Modersitzki J, Heldmann S, Wirtz S, Hömke L, Heide W, Kömpf D, Wree A. 2005. Three-dimensional cytoarchitectonic analysis of the posterior bank of the human precentral sulcus. *Anat Embryol* 210:387–400.
- Schmitt O, Modersitzki J, Heldmann S, Wirtz S, Fischer B. 2007. Image registration of sectioned brains. *Int J Comp Vis* 73:5–39.
- Schmitt O, Bethke S, Sobe P, Prehn S, Maehle E. 2008. Parallelized segmentation of a serially sectioned whole human brain. *Image Vis Comp* 26:289–301.
- Smart I, McSherry G. 1986a. Gyrus formation in the cerebral cortex in the ferret. I. Description of the external changes. *J Anat* 146:141–152.
- Smart I, McSherry G. 1986b. Gyrus formation in the cerebral cortex in the ferret. II. Description of the internal histological changes. *J Anat* 147:27–43.
- Toga A. 2002. Brain Mapping. The Methods. Amsterdam: Academic Press.
- van de Weijer J, van Vliet LJ, Verbeek PW, van Ginkel M. 2001. Curvature estimation in oriented patterns using curvilinear models applied to gradient vector fields. *IEEE Trans Pattern Anal Mach Intell* 23:1035–1042.
- Vogt C, Vogt O. 1919. Allgemeine Ergebnisse unserer Hirnforschung. *J Psychol Neurol* 25:279–461.
- von Economo C, Koskinas G. 1925. Die Cytoarchitektonik der Hirnrinde des erwachsenen Menschen. Berlin: Springer.
- von Economo C, Koskinas G, Triarhou L. 2007. Atlas of cytoarchitectonics of the adult human cerebral cortex. Karger, Basel.
- Walters N, Eickhoff S, Schleicher A, Zilles K, Amunts K, Egan G, Watson J. 2007. Observer-independent analysis of high-resolution mr images of the human cerebral cortex: In vivo delineation of cortical areas. *Hum Brain Mapp* 28:1–8.
- Weickert J. 1997. A review of nonlinear diffusion filtering. In: Scale-space theories in computer vision. Goos G, Hartmanis J, van Leeuwen J, Editors. Springer Berlin, New York. pp. 3–28.
- Weickert J. 1998. Anisotropic diffusion in image processing. Teubner, Stuttgart.
- Weickert J. 1999. Coherence-enhancing diffusion filtering. *Int J Comp Vis* 31:111–127.
- Zilles K, Palomero-Gallagher N. 2001. Cyto-, myelo-, and receptor architectonics of the human parietal cortex. *NeuroImage* 14:S8–S20.
- Zilles K, Schlaug G, Matelli M, Luppino G, Schleicher A, Qu M, Dabringhaus A, Seitz R, Roland P. 1995. Mapping of human and macaque sensorimotor areas by integrating architectonic, transmitter receptor, mri and pet data. *J Anat* 187:515–537.
- Zilles K, Palomero-Gallagher N, Schleicher A. 2004. Transmitter receptors and functional anatomy of the cerebral cortex. *J Anat* 205:417–432.
- Zilles K, Schlaug G, Geyer S, Luppino G, Matelli M, Schleicher A, Schormann T. 1996. Anatomy and transmitter receptors of the supplementary motor areas in the human and nonhuman primate brain. *Adv Neurol* 70:29–43.